Science Signaling
AAAS

www.sciencesignaling.org/cgi/content/full/5/247/ra77/DC1

Supplementary Materials for

Akt Phosphorylates the Transcriptional Repressor Bmi1 to Block Its Effects on the Tumor-Suppressing *Ink4a-Arf* Locus

Yan Liu,* Fan Liu, Hao Yu, Xinyang Zhao, Goro Sashida, Anthony Deblasio, Michael Harr, Qing-Bai She, Zhenbang Chen, Hui-Kuan Lin, Silvana Di Giandomenico, Shannon E. Elf, Youyang Yang, Yasuhiko Miyata, Gang Huang, Silvia Menendez, Ingo K. Mellinghoff, Neal Rosen, Pier Paolo Pandolfi, Cyrus V. Hedvat, Stephen D. Nimer*

*To whom correspondence should be addressed. E-mail: liu219@iupui.edu (Y.L.); snimer@med.miami.edu (S.D.N.)

Published 23 October 2012, *Sci. Signal.* **5**, ra77 (2012)
DOI: 10.1126/scisignal.2003199

The PDF file includes:

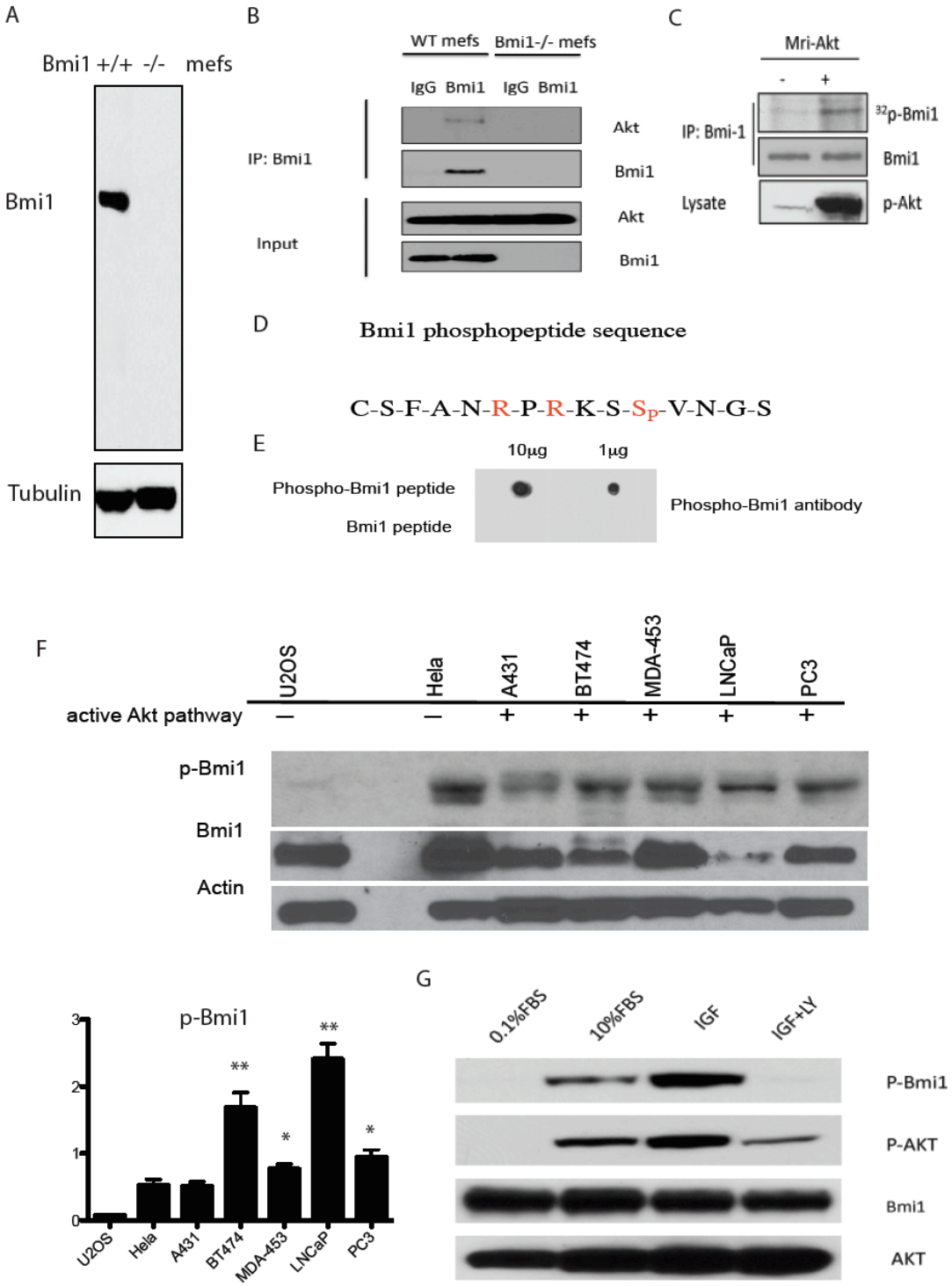
A
Bmi1 +/+ -/- mefs
Bmi1
Tubulin
B
WT mefs
Bmi1-/- mefs
IgG Bmi1 IgG Bmi1
IP: Bmi1
Akt
Bmi1
Input
Akt
Bmi1
C
Mri-Akt
- +
IP: Bmi-1
32p-Bmi1
Bmi1
Lysate
p-Akt
D
Bmi1 phosphopeptide sequence
C-S-F-A-N-R-P-R-K-S-Sp-V-N-G-S
E
10μg 1μg
Phospho-Bmi1 peptide
Bmi1 peptide
Phospho-Bmi1 antibody
F
U2OS Hela A431 BT474 MDA-453 LNCaP PC3
active Akt pathway
– – + + + + +
p-Bmi1
Bmi1
Actin
p-Bmi1
3
2
1
0
**
**
*
*
U2OS Hela A431 BT474 MDA-453 LNCaP PC3
G
0.1%FBS
10%FBS
IGF
IGF+LY
P-Bmi1
P-AKT
Bmi1
AKT

Figure S1. Akt phosphorylates Bmi1 in cells. (A) Western blot analysis of Bmi1 abundance, using wild-type and Bmi1 null MEFs, to show the specificity of the anti-Bmi1 antibody. (B) Bmi1 associates with endogenous Akt in cells, as indicated by immunoprecipitation and Western blotting in MEFs (n = 3 sets of cells). (C) Akt phosphorylates Bmi1 in cells. Bmi1 phosphorylation was determined by phospho-labeling. (D) The sequence of the Bmi1 phosphopeptide used for antibody production. (E) The specificity of the phospho- (Ser^{316})-Bmi1 antibody was shown using a dot blot analysis. The phospho-specific (Ser^{316})-Bmi1 antibody recognizes the phospho-Bmi1 peptide, but not the nonphosphorylated Bmi1 peptide. (F) Two cell lines (U2OS and HeLa cells) without and five cell lines (A431, BT474, MDA-453, LNCaP, and PC3 cells) with an active Akt pathway were used. The ratio of p-Bmi1 to Bmi1 was calculated based on densitometry. The graph shows the amount of phosphorylated Bmi1 normalized to total Bmi1. $^{**}P < 0.001$ compared to U2OS cells by one-way analysis of variance (ANOVA) and Bonferroni's post hoc test. (G) U2OS cells were serum-starved for 36 hours prior to serum or IGF exposure, in the presence or the absence of the PI3K inhibitor LY294002 (LY). Bmi1, p-Bmi1, Akt and p-Akt antibodies were used for Western blot analysis. An anti-actin antibody was used to show equal protein loading. Data represent at least three independent experiments.

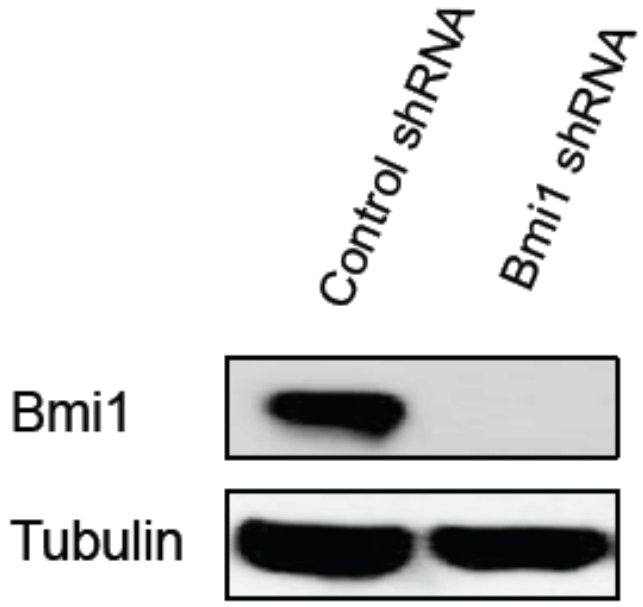

Figure S2. Knockdown of Bmi1 in wild-type MEFs with RNA interference.
(A) Efficient knockdown of Bmi1 in wild-type MEFs using RNAi. Data represent at least three independent experiments.

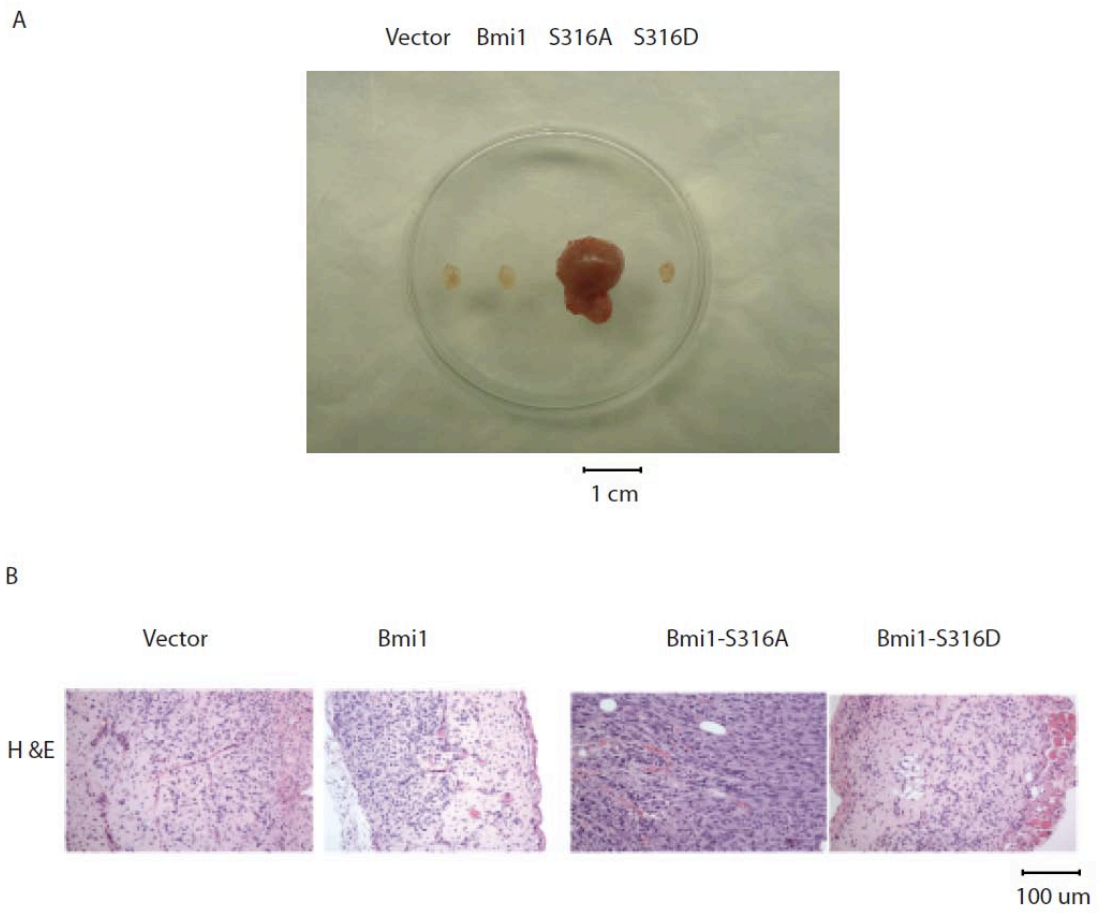

Figure S3. The Bmi1-S316A mutant enhances tumor formation in nude mice. (A) Actual size of tumors measured by photograph taken six weeks after injection. (B) Histopathological analysis of tumors formed in nude mice from *p53*$^{-/-}$ MEFs transduced with empty vector, or a vector that express wild-type Bmi1 or the S316A and S316D mutant proteins. H&E, hematoxylin-eosin. Data represent at least three independent experiments.

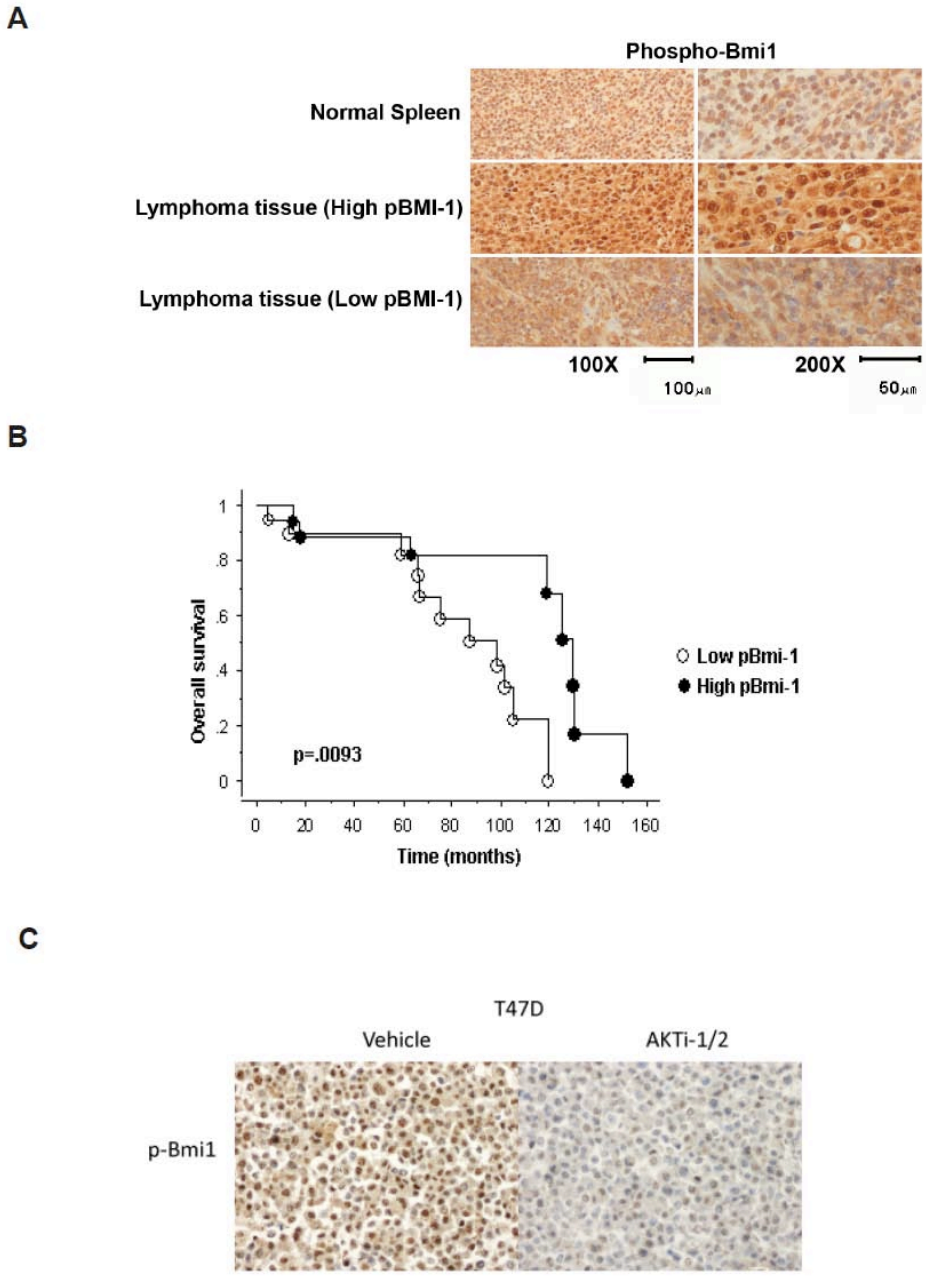

Figure S4. Phosphorylated Bmi1 is detectable in human diffuse large B cell lymphoma samples. (A) Phosphorylation of Bmi1 in human lymphoma patient samples (and normal spleen) was determined by immunohistochemistry using a phospho (Ser^{316})-specific anti-Bmi1 antibody. High pBmi1 (n=21 samples) indicates a degree of staining above the median intensity and low pBmi1 (n=21 samples) indicates a degree of staining below the median intensity. (B) Correlation between phosphorylation of Bmi1 and the survival of patients with human diffuse large B cell lymphoma. A total of 42 patient samples were used. (C) Detection of phospho-Bmi1 in T47D cells in the presence and absence of the AKT inhibitor AKTi-1/2, using a phospho (Ser^{316})-specific anti-Bmi1 antibody for immunohistochemistry. Data represent three independent experiments.

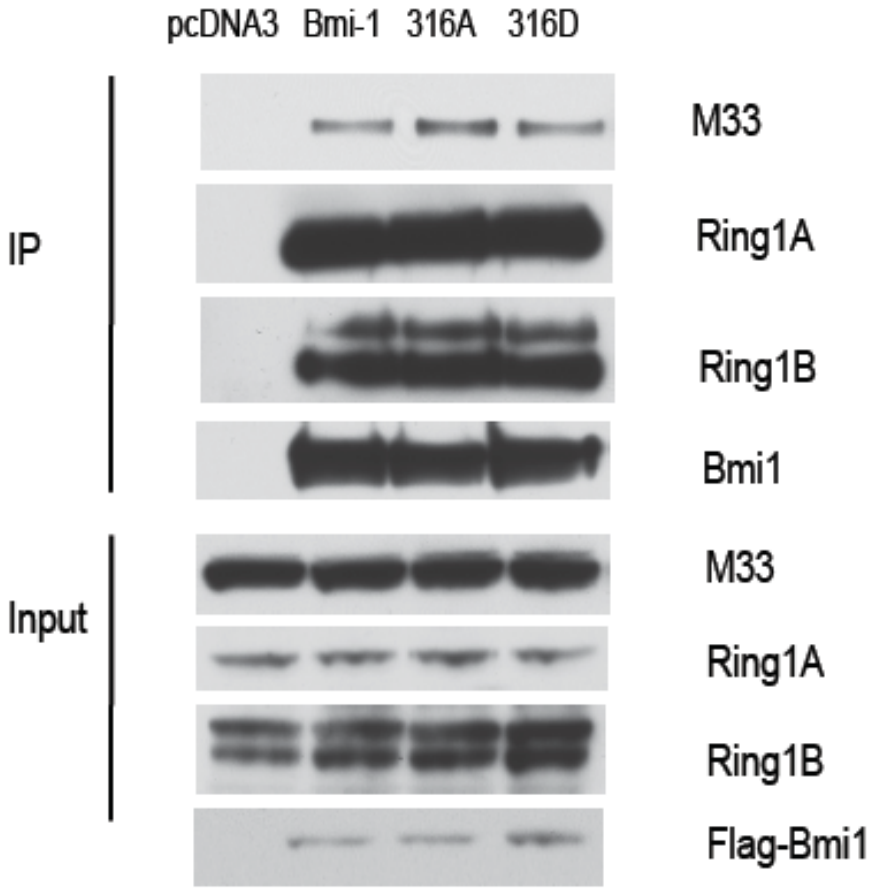

Figure S5. The PI3K-Akt signaling pathway does not affect PRC1 complex formation. (A) Coimmunoprecipitation of wild-type or mutant Bmi1 and various components of the PRC1 complex. Lysates were prepared from 293T cells transfected with Flag-tagged wild-type Bmi1, S316A or S316D mutant proteins, immunoprecipitated with anti-Flag antibodies and blotted with anti-Ring1B, anti-Ring1A, anti-M33 and anti-Flag antibodies, respectively. Data represent three independent experiments.

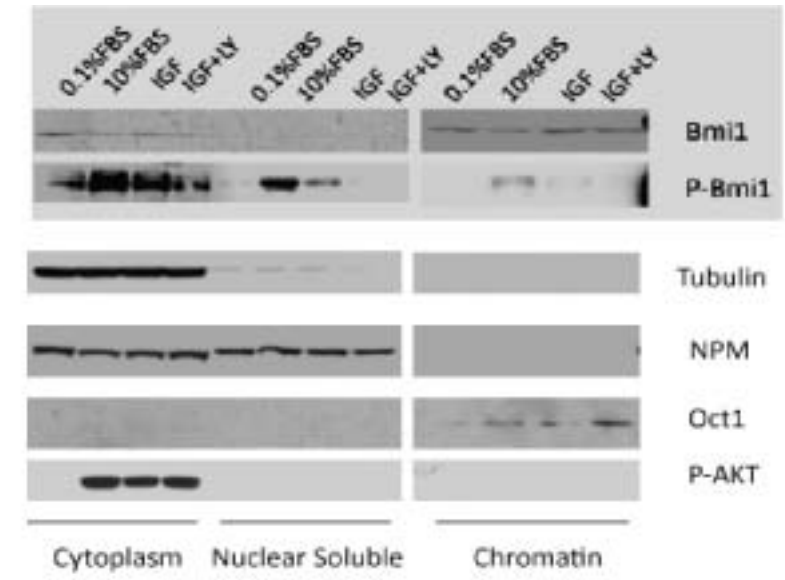
0.1%FBS
10%FBS
IGF
IGF+LY
Bmi1
P-Bmi1
Tubulin
NPM
Oct1
P-AKT
Cytoplasm
Nuclear Soluble
Chromatin

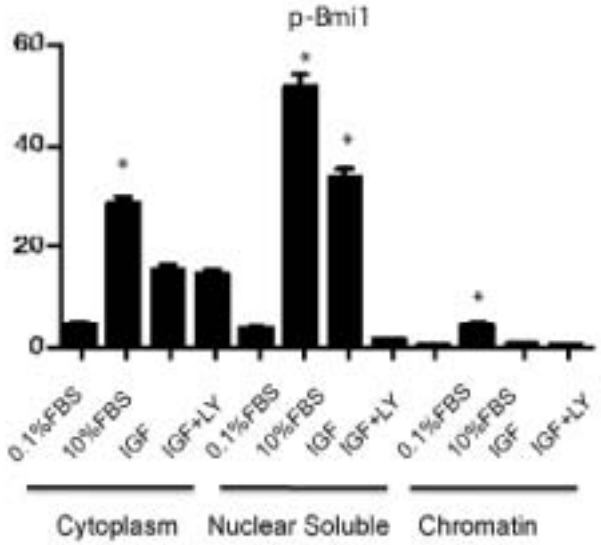
p-Bmi1
60
40
20
0
0.1%FBS
10%FBS
IGF
IGF+LY
Cytoplasm
Nuclear Soluble
Chromatin

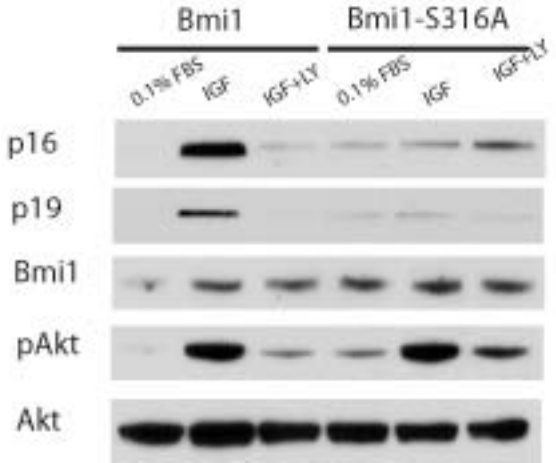
Bmi1
Bmi1-S316A
0.1% FBS
IGF
IGF+LY
p16
p19
Bmi1
pAkt
Akt

Figure S6. Subcellular localization of Bmi1 in U2OS cells after serum or IGF exposure. (A) U2OS cells were serum-starved for 36 hours prior to serum or IGF exposure, in the presence and absence of the PI3K inhibitor LY294002 (LY) and then subjected to cell fractionation. Western blot analysis demonstrates the increase in phospho-Bmi1, which is found primarily in the cytoplasmic and to a lesser degree the nuclear soluble fraction of the cells. A small amount of phospho-Bmi1 is found in the chromatin-bound fraction following 10% FBS stimulation. The graph shows the amount of phosphorylated Bmi1 normalized to total Bmi1. *P< 0.01 compared to serum-starved U2OS cells by (ANOVA) and Bonferroni's post hoc test. (B). IGF treatment triggers the phosphorylation of wild-type Bmi-1, but not the S316A mutant, alleviating repression of the *p16* and *p19* genes in wild-type MEFs, as determined by Western blot analysis. Data represent three independent experiments.

A

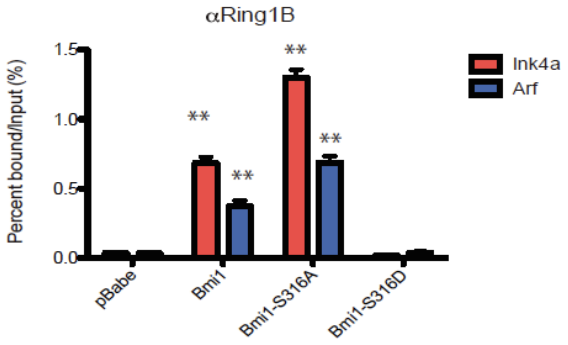

B

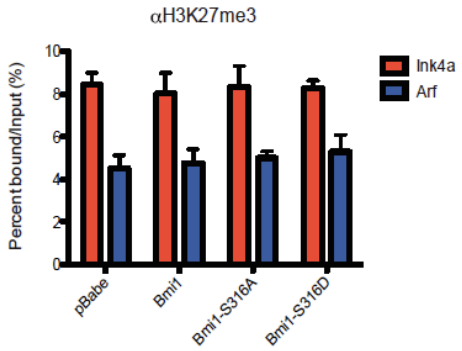

C

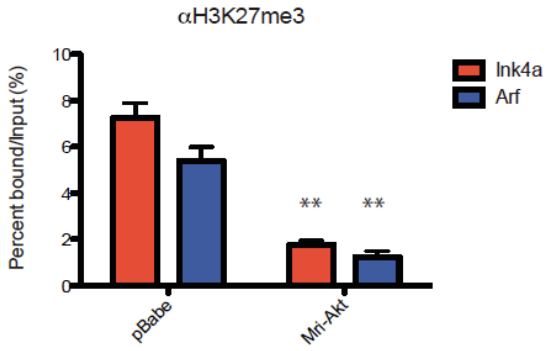

Figure S7. ChIP assays of the *Ink4a-Arf* locus in MEFs. (A). ChIP analysis of the *Ink4a-Arf locus* using Ring1B antibody and cells shown in Figure 6A. ***P*< 0.001 compared with pBabe-transduced MEFs by two-way ANOVA, n = 3 independent experiments. (B) ChIP analysis of the *Ink4a-Arf* locus using an anti-H3K27me3 antibody and cells shown in Figure 6E. (C) ChIP analysis of the *Ink4a-Arf* locus using an anti-H3K27me3 antibody and cells shown in Figure 6A. ***P*< 0.001 compared with pBabe transduced MEFs by two-way ANOVA, n = 3 independent experiments.